Optical Materials 122 (2021) 111685

Contents lists available at ScienceDirect

Optical Materials

journal homepage: www.elsevier.com/locate/optmat

Investigation of nitrogen doped ZnO thin films: Effects on their structural and optical properties

H. Hopoğlu [a], H.S. Aydınoğlu [b], A. Özer [c,d], E. Şenadım Tüzemen [e,f,*]

[a] Faculty of Technology, Department of Optical Engineering,Sivas Cumhuriyet University, 58140, Sivas, Turkey
[b] Department of Medical Services and Techniques, Program of Opticianry, Vocational School of Healthcare, Sivas Cumhuriyet University, 58140, Sivas, Turkey
[c] Department of Metallurgical and Materials Engineering, Sivas Cumhuriyet University, 58140, Sivas, Turkey
[d] Advanced Technology R&D Center, Sivas Cumhuriyet University, 58140, Sivas, Turkey
[e] Nanophotonics Research and Application Center, Sivas Cumhuriyet University, 58140, Sivas, Turkey
[f] Department of Physics, Faculty of Science, Sivas Cumhuriyet University, 58140, Sivas, Turkey

ARTICLE INFO

Keywords:
N doped ZnO
Magnetron sputtering
Spectroscopic Ellipsometer
XRD
Energy band gap

ABSTRACT

Un-doped and nitrogen-doped ZnO thin films were grown by using radio frequency (RF) magnetron sputtering method changing the nitrogen flow rate between 0% −12.5% and the thickness dependence of films was determined. The effect of nitrogen doping concentration on the structural, morphological, and optical properties of zinc oxide thin films was studied. X-ray diffraction (XRD) analysis confirmed that the nitrogen-doped ZnO films belong to the hexagonal crystal structure. The optical properties of the grown samples were examined by optical spectrophotometer and spectroscopic ellipsometer. Transmittance spectra were obtained by spectrophotometer measurements and the effect of nitrogen ratio was investigated. It has been observed that as the nitrogen ratio increases, the transmittance decreases up to ~500 nm and then increases. By using the transmittance curve, the energy band gap was calculated. Further detailed optical analysis was made by the spectroscopic ellipsometry technique. Fitting was performed to ensure the agreement between the experimentally obtained Ψ values and theoretically determined Ψ values using the Cauchy model. As a result, the refractive index was found for each film and it was observed that the refractive index decreased as the nitrogen ratio increased. The scanning electron microscopy (SEM) measurements showed that the surface morphology of the films changes with N doping. Nitrogen was observed in Fourier transform infrared spectra analysis. 5% nitrogen-doped ZnO films were grown on the glass substrate using RF magnetron sputtering at room temperature. Samples are prepared by varying thicknesses during the deposition process. XRD and SEM measurements of the samples show the variation in the crystal structure and surface morphology of the film with varying thicknesses. All the samples are tested for the transmittance and band gap. The increase of film thickness increases the grain size. The transmittance is influenced by the film thickness.

1. Introduction

Metal oxides (MO) thin films can be used in various fields due to their extraordinary properties such as wide band gaps, good electrical conductivity, optical transmittance, and high reflectivity in the infrared (IR) region. MO thin films are the coating layers with wide application areas such as electronics, magnetism, optical and solar energy conservation, batteries and photovoltaic materials, gas and moisture sensors, and optoelectronics [1]. The benefit of using MOs is that their chemical and electronic properties can be adjusted to allow charge exchange with a wide variety of organic/inorganic molecules [2].

Zinc oxide (ZnO) is one of the most important metal oxides, which do not contain toxic substances, is environmentally friendly, easily accessible, convenient, and cost-effective [3]. ZnO is a direct band gap natural n-type semiconductor with a wide band gap value (~3.3 eV) that has a high exciton binding energy (60 meV) [4,5]. Due to its wide band gap, it is accepted as a suitable material for LED construction in the blue and ultraviolet regions of the electromagnetic wave spectrum [6]. It has many application in technology such as; acoustic wave (SAW) devices, gas sensors, organic wastewater treatment, layers of photovoltaic cells, photodetectors, various electronic and optoelectronic devices, biosensors, flat panel display, light-emitting diodes, flexible or wearable UV

* Corresponding author. Nanophotonics Research and Application Center, Sivas Cumhuriyet University, 58140, Sivas, Turkey.
E-mail address: esenadim@cumhuriyet.edu.tr (E. Şenadım Tüzemen).

https://doi.org/10.1016/j.optmat.2021.111685
Received 10 September 2021; Received in revised form 7 October 2021; Accepted 9 October 2021
Available online 13 October 2021

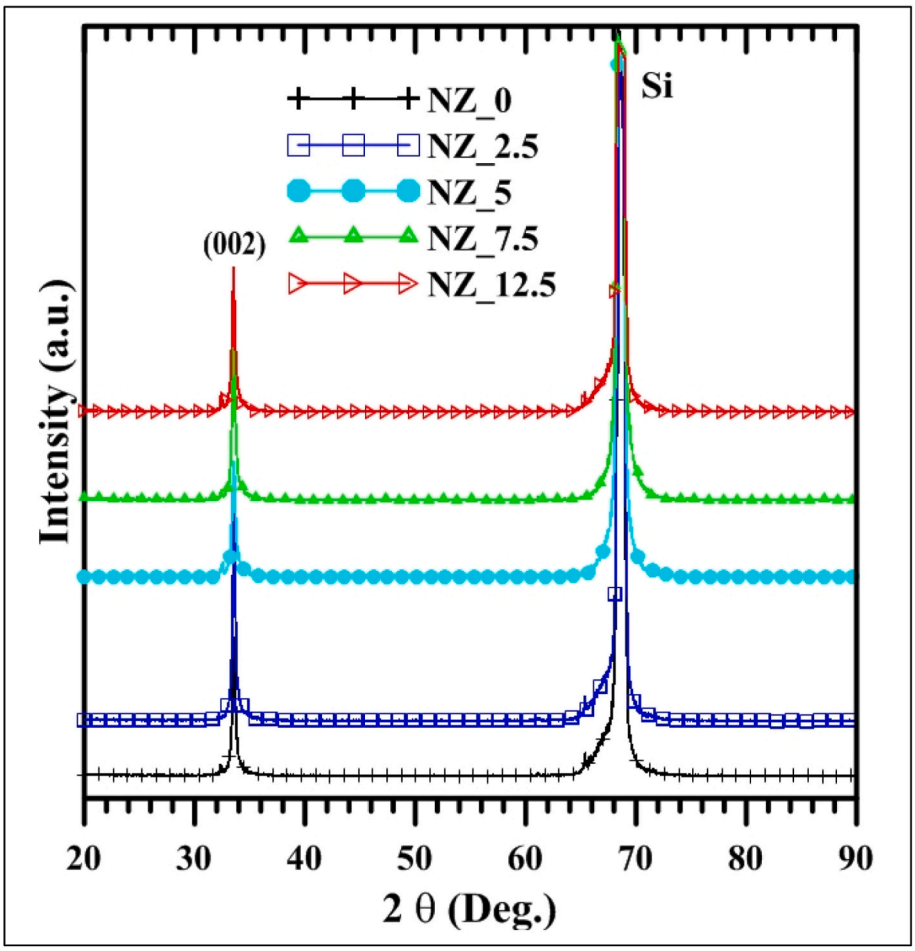

Fig. 1. XRD graphics of the samples deposited on n-Si.

Table 1
The films with varying nitrogen flow rate for 250 nm thickness.

		NZ_0	NZ_2.5	NZ_5	NZ_7.5	NZ_12.5
Ar	%	100	97.5	95	92.5	87.5
	Sccm	2.5	2.3 ± 0.2	2.3 ± 0.2	2.2 ± 0.2	2.2 ± 0.1
N	%	0	2.5	5	7.5	12.5
	Sccm	0	0.1 ± 0.05	0.2 ± 0.05	0.3 ± 0.05	0.3 ± 0.05

Table 2
X-ray diffraction data results of samples deposited on n-Si.

	Angle (deg.)	Height	d (Å)	Assignment	FWHM (deg.)	D (nm)
NZ_0	33.49	1447	2.67	(002)	0.29	28.24
	68.59	143398	1.37	Si	0.11	
NZ_2.5	33.51	2139	2.67	(002)	0.27	31.33
	68.60	137685	1.37	Si	0.12	
NZ_5	33.49	1166	2.67	(002)	0.35	23.86
	68.61	172488	1.37	Si	0.13	
NZ_7.5	33.47	1721	2.68	(002)	0.31	27.13
	68.60	188724	1.37	Si	0.12	
NZ-12.5	33.46	1497	2.68	(002)	0.29	28.83
	68.59	131582	1.37	Si	0.11	

light sensors, spintronic devices, biomedical applications, and surfaces [7–12].

Doped and un-doped ZnO thin films can be prepared by various methods such as: chemical vapor deposition (CVD) [13], radio frequency (RF) magnetron sputtering [14], DC reactive magnetron sputtering [15], metal organic chemical vapor deposition (MOCVD) [16], molecular beam epitaxy (MBE) [17], pulsed laser deposition [18], sol-gel method [19], ultrasonic spray pyrolysis technique (USP) [20], sol-gel dip-coating technique [21], physical vapor deposition (PVD) [22], high power impulse magnetron sputtering (HiPIMS) [23], modified polymeric precursor (MPP) [24], hydrothermal [25], solvothermal [26,27], successive ionic layer adsorption and reaction (SILAR) method [28], microwave-assisted hydrothermal (MAH) [29–31], and free solvent [32,33].

There are many studies in which the properties of ZnO semiconductor thin films have been changed by adding metallic elements such as Cr, In, Ga, Si, Al, as well as non-metallic dopants such as F, N. Nitrogen has a similar radius and electrical structure to oxygen. So it is considered a promising candidate to produce a shallow acceptor level in ZnO. Nitrogen in the fifth group is believed to be a better dopant element for p-type conductivity in ZnO, which has the smallest ionization energy [34]. Nitrogen-doped films may provide high transmittance and low resistivity values. Earlier studies showed that In-doped ZnO thin films in amorphous structure showed better electrical properties than thin films in crystalline structure [35–37]. On the other hand, fluorine additives increased the crystallization of ZnO films and it has also reduced grain boundary scattering and the dual doping of F and Al is considered to be a reasonable method for obtaining higher performance transparent conductive ZnO films [38].

There are different publications in the literature on nitrogen-doped ZnO at low temperature. Nitrogen-doped ZnO films were produced on Corning Glass substrates with a low coefficient of expansion studied by Tu et al. [39]. These films produced by RF sputtering technique at room temperature (RT) were made by using Ar (20 sccm) as sputtering gas at

Table 3
N doping efficiency by increasing N concentration of device adjustment with elemental distribution.

	NZ_0		NZ_2.5		NZ_5		NZ_7.5		NZ_12.5	
Element	Wt%	At%	Wt%	At%	Wt%	At%	Wt%	At%	Wt%	At%
O K	17.31	46.11	20.44	50.16	18.35	45.16	17	43.25	18.54	45.31
Zn L	82.69	53.89	78.62	47.19	79.08	47.62	80.78	50.29	78.73	47.09
N K	–	–	0.94	2.65	2.57	7.22	2.22	6.46	2.72	7.6
N doping efficiency %	–	–		106		144.4		86.13		60.8
Thickness (nm)	235 ± 6		232.5 ± 5		241.7 ± 7.5		242 ± 5		246 ± 7	

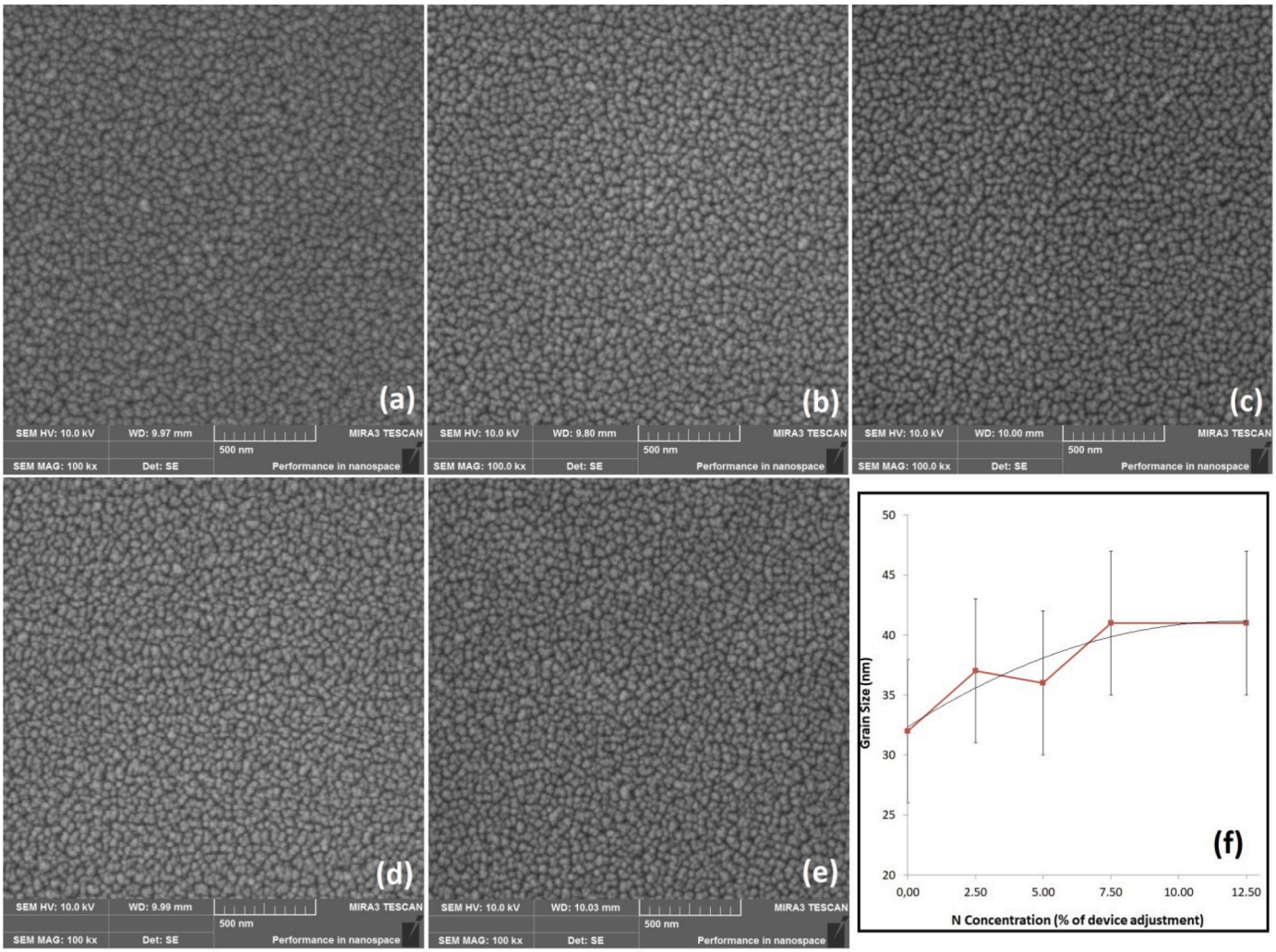

Fig. 2. SEM−SE surface topographies of **(a)** pure ZnO, **(b)** 2.5% N, **(c)** 5% N, **(d)** 7.5% N, **(e)** 12.5% N doping of 250 nm ZnO coating on Si, **(f)** grain size divergence graph of images.

200 W power, under 5 mTorr pressure and adding N_2 (6, 10, 15 sccm) to it at increasing flow rates. It was observed that the N/Zn atomic ratios decreased with increasing N_2 flow rate. The micro photoluminescence spectrum peaks were observed in the near-UV range [39]. Moreover, N-doped ZnO films were also produced by RF sputtering technique by applying different N_2/O_2 ratios on sapphire (0001) substrates at RT by Nie et al. [40]. As a result of this study, they observed that N-doped ZnO films exhibited both p-type conductivity and ferromagnetism [40]. Pathak et al. produced un-doped and N-doped ZnO films at 160 W power by using radio frequency (RF) reactive magnetron sputtering technique by applying different nitrogen ratios (5, 7, 10 sccm) on glass substrates. As a result of this study, it was seen that the film has a wurtzite hexagonal crystalline structure. Current-voltage properties of the doped films also showed p-type conductivity in N-doped thin films [41].

In the literature [39–41], it is rarely encountered that nitrogen-doped ZnO films work at low temperatures. For this reason, in order to eliminate the deficiencies related to this subject in the literature, ZnO was produced by doping with nitrogen, and its usability as a device was investigated by examining its optical properties. Optical properties, especially the spectroscopic ellipsometry method, have been studied in detail for samples produced at low temperature. As a result, it is thought to contribute to the literature about the refractive index. In addition, thanks to the morphological characterizations, one of the materials with the lowest surface roughness was obtained.

2. Experimental procedure

In this study, ZnO films were deposited in RF magnetron sputtering

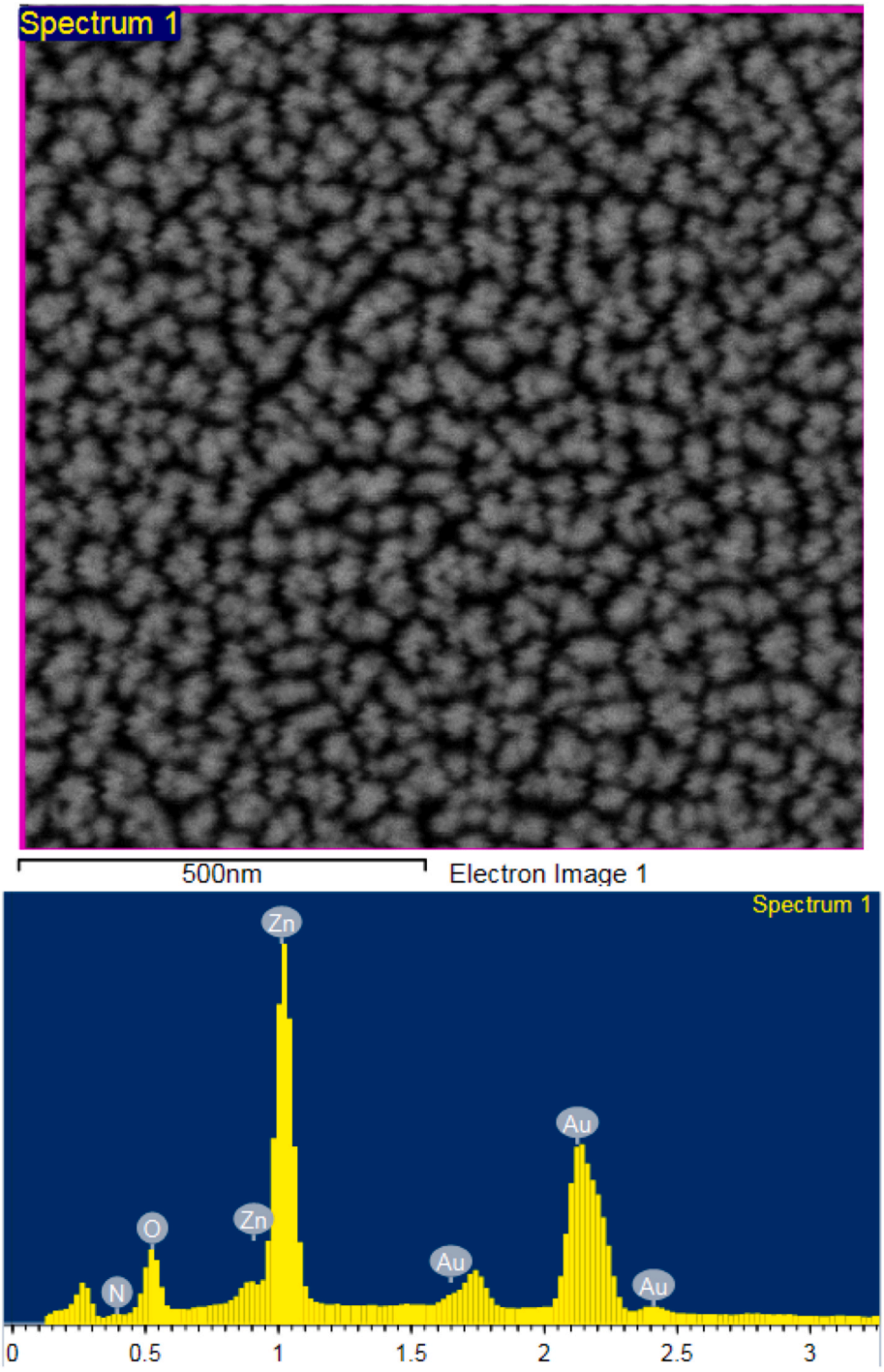

Fig. 3. SEM-EDX analysis of 5% N doping on ZnO and its spectrum.

system using a ZnO target at RT. NANOVAK NVTS-400-2TH2SP Thermal & Sputter Combined System was used to produce nitrogen-doped ZnO films. ZnO target was purchased from Plasmaterials Co. Inc. with a purity of 99.9% and with a thickness of 0.125 inches and 2 inches of diameter. Firstly, substrates were placed in acetone filled in a small glass beaker. Substrates were cleaned in acetone for 8–10 min and were left to dry. The distance between the target and the material to be coated was kept constant at 6.2 cm. During the film growth, the thickness of the films was measured with Angstrom precision with the help of a thickness monitor in the system. The base pressure before film deposition was approximately $\sim 10^{-6}$ Torr, and $\sim 5 \times 10^{-3}$ Torr was achieved. All films for plasma generation were done by applying 60 W power. The growth rate was 0.6 Å/s.

First, ZnO coatings were performed at different nitrogen flow rates on silicon and glass substrates. n-Si was chosen for measurement of refractive index and FTIR analysis while the glass substrate was chosen for transmittance and energy bad gap measurements. All films were deposited to be 250 nm thick on both substrate materials. N doping was abbreviated as NZ thereafter and the flow rate was chosen as 0, 2.5, 5, 7.5 and 12.5 and coded at the end of NZ such as NZ_2.5 for 2.5% N flow rate. Then, four different films were grown on glass substrates at 5% nitrogen flow rate being constant with thicknesses of 250, 350, 450 and 550 nm.

Characterizations of the samples were performed by the techniques

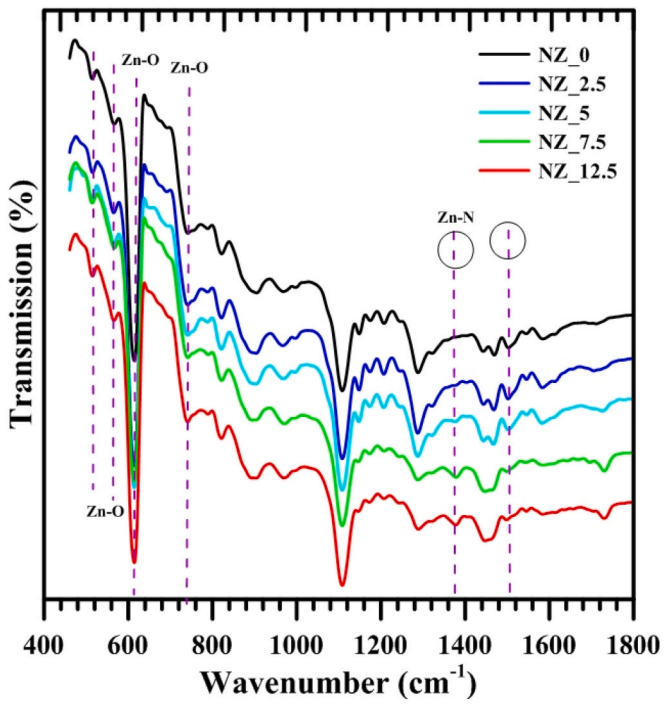

Fig. 4. FTIR analysis of N doped ZnO thin films.

as following: Crystal structures of the samples were examined by θ-2θ scan in Rigaku Miniflex II Desktop X-ray Diffractometer system was used with Cu Kα radiation (λ = 1.54059 Å). Diffraction was obtained in the range of 2θ = 20–90°. The surface morphology of the samples was determined by scanning electron microscopy (TESCAN® MIRA3 XMU (Brno, Czechia) at an accelerating voltage of 10 kV). Optical characterization of the samples was carried out using a double-beam UV–Vis–NIR spectrophotometer (Cary 5000). Optical transmission of samples was taken in the wavelength range of 280–700 nm using a solid sample holder accessory. Fourier Transform Spectroscopy (FTIR) analyzed with Bruker Model: Tensor II. Thickness of the samples are probed by OPT-S9000 Spectroscopic Ellipsometry. The measurements were made in the wavelength range of 375–1000 nm with a step size of 3 nm and at angles of incidence of 70°.

3. Results and discussion

3.1. Nitrogen doping concentration of films

3.1.1. X-ray diffraction

In Fig. 1, the crystal structures of ZnO thin films doped with different nitrogen percentages on silicon are shown by X-ray diffraction (XRD). X-ray measurements were made in the range of 20–90° with 0.02°/steps. Accordingly, it was observed that the films were ZnO with especially (002) orientations which can be concluded as the orientation dependence of growth hexagonal structures by nitrogen doping [42]. The possible fluctuations in N flow rate can affect the growth of hexagonal type ZnO and possibly favor the elongation of ZnO wurtzite in c axis.

The grain size in the films is calculated from the X-ray diffraction data by using the well-known Scherrer formula [43];

$$D = \frac{K\lambda}{\beta \cos\theta} \tag{1}$$

where $\boldsymbol{K}$ is a geometrical constant, λ is the wavelength of the X-ray used, $\boldsymbol{\theta}$ is the Bragg reflection angle, and $\boldsymbol{\beta}$ is the half-maximum width (FWHM) of the reflections in radians. For calculations, $\boldsymbol{K}$ and λ constants were taken as 0.90 and 0.154 nm, respectively (see Table 1).

In ZnO thin films doped with different nitrogen percentages, it was observed that the $2\boldsymbol{\theta}$ angle shifted as the nitrogen percentage increased (except for zero). As seen in Table 2, the particle size first increased, then decreased, and then increased again for the (002) orientation. These results showed that it behaves in harmony with the particle size measured in FWHM and SEM. These results also may be attributed to the N doping into ZnO structure by elongating c axis while the axis becomes narrower due to the atomic radius of N versus O and Zn. The efficiency of N doping of 5% can be said to be the best among the concentrations by better penetration possibility of N as can be seen later in Table 3.

3.1.2. SEM of structure

SEM analyses were performed on surfaces at 10 kV with a working distance of 9 mm. Secondary electron (SE) imaging was employed to see better quality photos of the surface, no BSE (backscattered electron imaging) was not used since the surfaces do not provide any phases other than ZnO.

As clearly be seen from Fig. 2, the spherical grain size morphology were observed in all samples. This could be attributed to the formation of a good sputter regime and energy within the substrate and ZnO

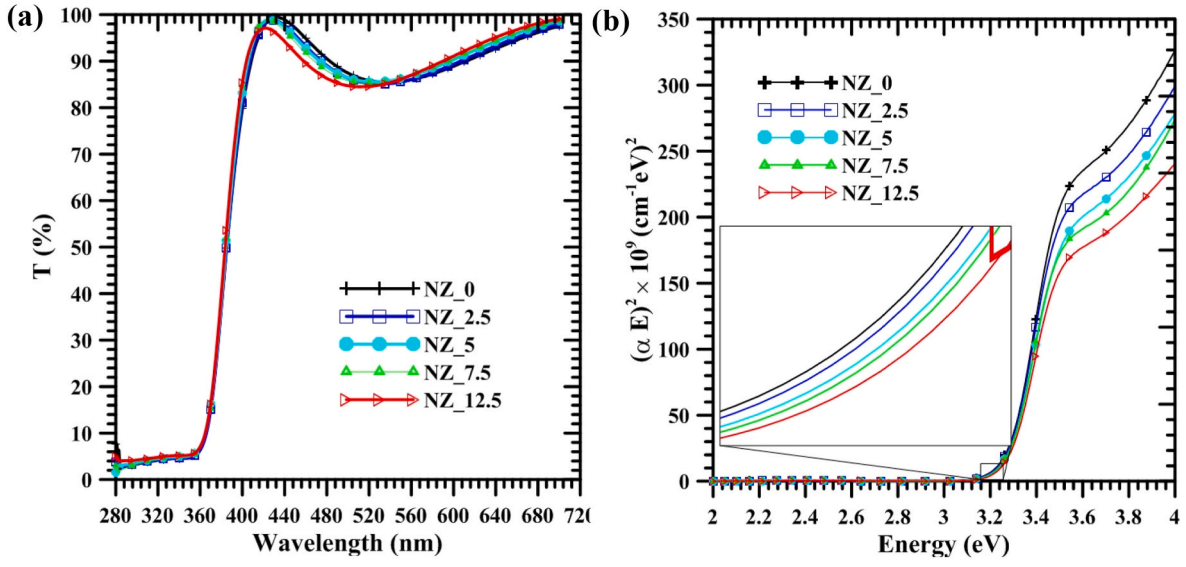

Fig. 5. a) Transmittance spectra **b)** the plot of $(\alpha h\upsilon)^2$ against the photon energy $h\upsilon$ to calculate the bandgap energy.

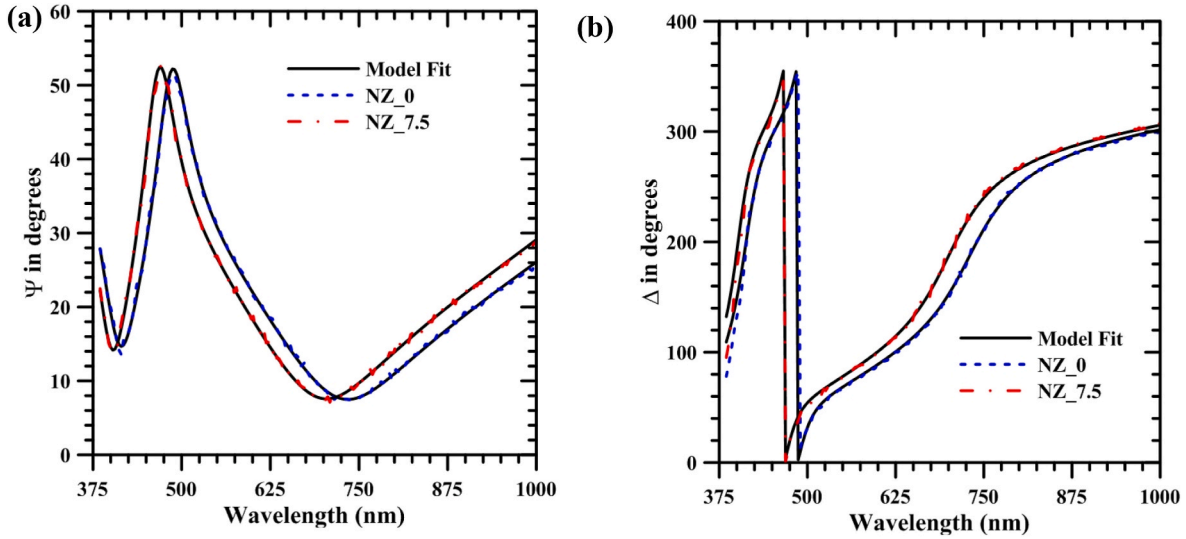

Fig. 6. The spectral dependence of Ψ and Δ for nitrogen flow rate 0% and 7.5%. The experimental data obtained and modeling curves are shown.

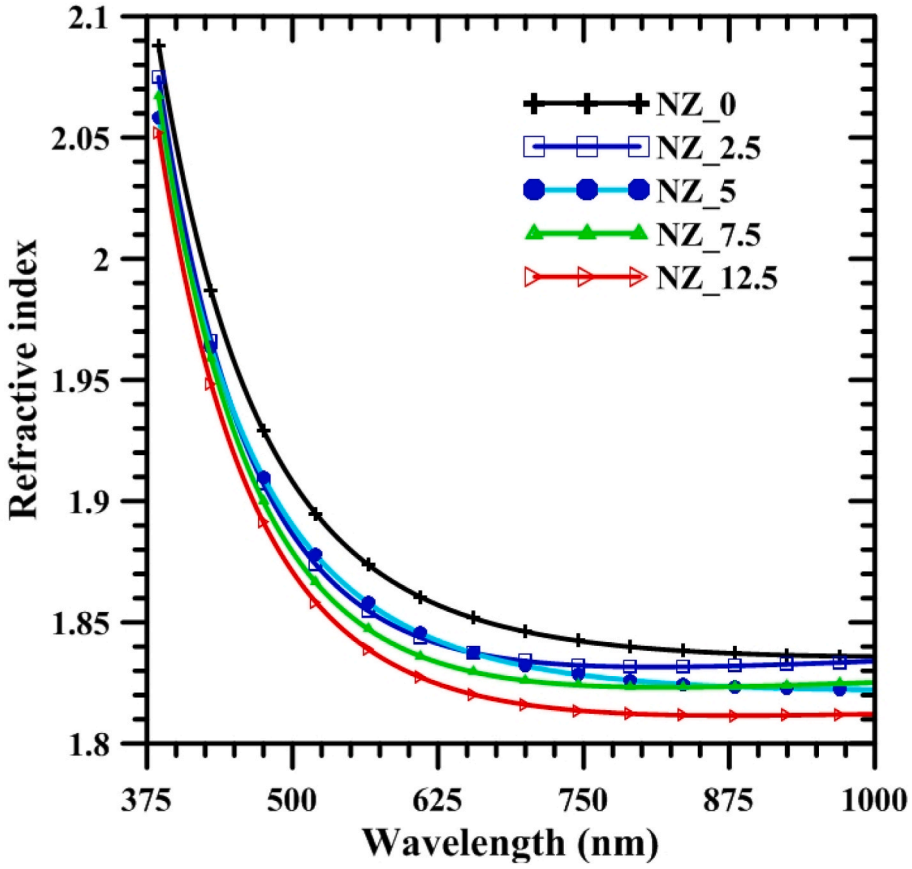

Fig. 7. At various nitrogen flow rates refractive index vs. wavelength plots.

Table 4
Elipsometer MSE and elipsometer thickness (nm) values for all samples.

	NZ_0	NZ_2.5	NZ_5	NZ_7.5	NZ-12.5
Elipsometer MSE	4.92	12.14	10.91	6.51	7.81
Elipsometer Thickness (nm)	234.1 ± 0.348	235.1 ± 0.332	235.2 ± 0.362	235.5 ± 0.362	235.8 ± 0.374

accompanied by N doping. From **(a)** to **(e)**, by increasing N doping, a slight increase in grain size from 32 ± 5 nm to 41 ± 6 nm should be considered. Besides, there is a standard deviation of around 6 that may be concluded as the continuous spherical morphology of grains but some coarsening occurred by N penetration to crystal structure. N has a smaller atomic radius than others and can standstill as the interstitial among Zn–O atoms and their octahedral and tetrahedral coordination occupancy. From Fig. 3, EDX elemental analysis (at 8 kV) of surface

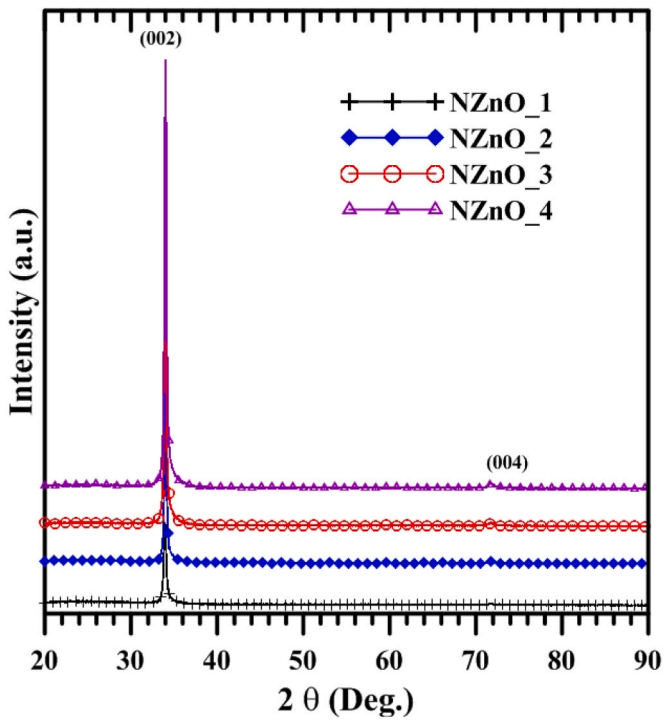

Fig. 8. The X-ray diffraction spectra of thin films with different thickness.

Table 5
X-ray diffraction data results table of samples produced on glass.

	Angle (deg.)	Height	d (Å)	Assignment	FWHM (deg.)	D (nm)
NZnO_1	33.89	2589	2.64	(002)	0.28	30.11
	71.77	26	1.31	(004)	0.71	13.82
NZnO_2	33.96	5808	2.64	(002)	0.22	37.79
	71.88	53	1.31	(004)	0.65	15.11
NZnO_3	33.91	8369	2.64	(002)	0.23	35.67
	71.77	90	1.31	(004)	0.55	17.84
NZnO_4	33.96	15013	2.64	(002)	0.20	41.56
	71.73	156	1.31	(004)	0.56	17.52

topography, N doping efficiency was found to be 106% of actual device adjustment for 2.5% N doping which has a tendency of decreasing down to 61% of 12.5% N doping by device adjustment. In the beginning, Zn:O ratio was very close for pure coating as 54:46, but then by increasing N ratio, Zn:O ratio has been similar with the stoichiometry which was about 47:45 at the 12.5% N. This phenomenon can also be attributed to the collision of N with Zn and O elements to form a 1:1 atomic ratio of ZnO phase. N can also scatter especially O atom to form a possible formula of NO or NO_x which goes to vacuum and alters the sputter of 1:1 ZnO coating on the surface.

In Table 3, N doping efficiency can be also concluded in this stage. This means that the adhesion performance of N increases up to 5% then drastically decreases down to 61%. This process may be due to the increasing coating thickness, so N cannot stick on the surface of ZnO even into the crystal structure by decreasing nanoparticle area that increases from 32 nm to 41 nm by increasing N content.

3.1.3. FTIR analysis

Fig. 4 represents the FTIR analysis for thin films of ZnO produced by different N amounts between 460 and 1800 cm^{-1}. As seen in spectrums, all materials are seen as similar with some differentiations. Especially the peaks at ~1380 and ~1502 cm^{-1} attributed to Zn–N bonds which appeared with increased N doping. The peak at 1502 cm^{-1} first increased and then decreased after a certain amount of N, but in fact, that peak overlaps with Zn–O bonds. After 5% N doping, Zn–O bonding was disappeared and Zn–N peak remained instead. Since N is a very small atom and the interaction and distance for atomic bondings are very short, then N–O, Zn–N, and Zn–N–O stretching are seen as very broad and weak peaks as in literature [44,45].

The peak was identified at ~512.06 cm^{-1} due to vibrational modes of Zn–O bond. In addition to that, the peak observed at ~570.54 cm^{-1} was the corresponding Zn–O bond (A1(LO)) stretching vibrational mode [45,46]. The observed peaks in ~741 to ~614 cm^{-1} indicate the stretching vibrations of ZnO [47].

3.1.4. Optical properties

To determine the optical properties of films, the films were grown on glass substrates. The transmittance graphs of samples were given in Fig. 5 (a). As the spectra were overviewed for films, by increasing N doping, the transmittance values around 500 nm were first decreased then increased, than decreased back to around zero.

Tauc formula [48] was used for calculating the energy band gap of produced films:

$$(\alpha h\nu)^2 = \left(h\nu eE_g\right). \tag{2}$$

Here, α; absorption coefficient, $h\nu$; photon energy, E_g; band gap and A; is a constant. The linear transaction of this plot for $(\alpha h\nu)^2 = 0$ is the energy gap value, the energy value of this point gives the semiconductor band gap.

The inset plot in Fig. 5 (b) shows zoomed area around 3.2 eV and the band gap values were decreased with increasing N doping into ZnO films. Depending on the change at Fermi level and carrier concentration, the conduction band was approached and low energy transitions were blocked and the energy gap changes. This phenomenon is known as the Burstein-Moss effect [49,50] by doping.

With ellipsometry technique, we can investigate the film thickness, refractive index, extinction coefficient, crystal quality, compositional variations, depth, and microstructural features. In this study, the film thickness and refractive index were found using ellipsometry technique which is based on the measurements of complex Fresnel reflection coefficient (ρ) ratios. Complex reflection ratio Ψ and Δ can be described as follows [51,52]:

$$\rho = \frac{\widetilde{R}_p}{\widetilde{R}_s} = \tan\Psi e^{i\Delta} \tag{3}$$

Here, $\tan(\psi)$ is the amplitude ratio on the reflection coefficient and Δ is the phase shift. In this study, by spectroscopic ellipsometry, all samples were measured as a function of wavelength. After measurements, the data were analyzed for determining the refractive index and film thickness. For the calculation of the measurements, Cauchy model was used [51]. For the fit from the model, the values at a spectral range that material wavelength was used for Cauchy layer *A, B, C* coefficients and estimated thickness were entered. Cauchy model can be described as follows [51,53]:

$$n = n_\infty + \frac{A}{\lambda^2} + \frac{B}{\lambda^4} \tag{4}$$

In Fig. 6 (a), the changes of ψ and **6 (b)** of Δ according to wavelength are shown theoretically and experimentally. Although the fit was made for all samples, only two samples were plotted to avoid graphical complexity.

Fig. 7 shows the variation of the refractive index according to the wavelength. It is noteworthy that the refractive index values of ZnO films decrease with the introduction of nitrogen into the structure. It is thought that the decrease in the packing density of the grains in nitrogen-doped ZnO films may cause a decrease in the refractive index values. In addition, the MSE and thickness values obtained as a result of the fit are shown in Table 4.

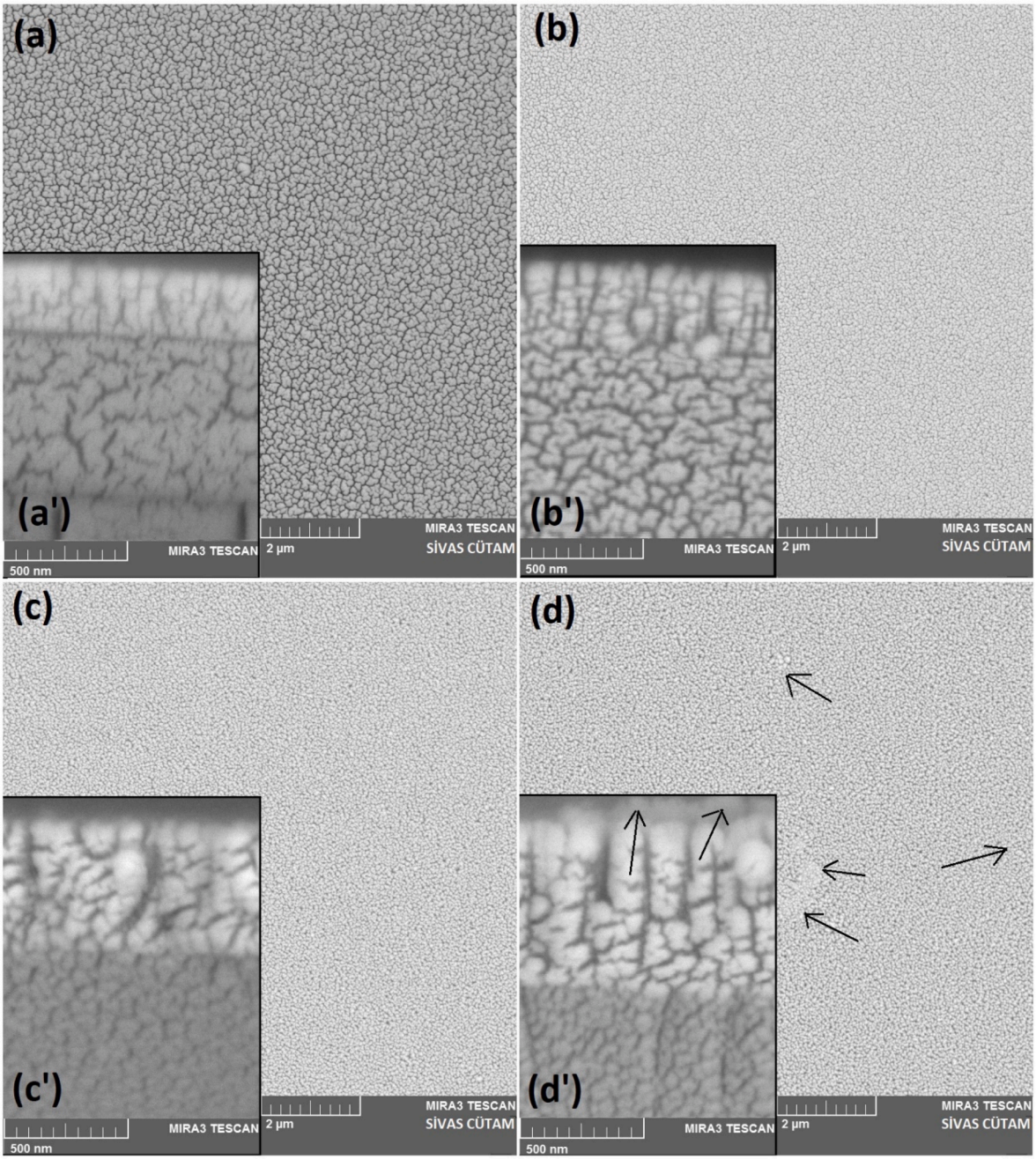

Fig. 9. SEM images of N-dopped ZnO films (a) 250 nm, (b) 350 nm, (c) 450 nm, (d) 550 nm.

3.2. The thickness dependence of films

3.2.1. X-ray diffraction

In Fig. 8, the XRD analyses of ZnO-coated samples on glass with 5% N doping were evaluated. As seen clearly from Fig. 8, (002) preferred orientation was found in ZnO-coated samples. There are some small peaks that were attributed to (004) orientation but these peaks are relatively short hat may be due to the single crystal orientation dependence of ZnO blocks to be seeded and grown.

As tabulated in Table 5, the height of (002) peaks is more than (004) peaks that make them single-crystal favorable, those peaks can form even due to the faster growth possibility and seeds that buckled or bent to any side while growing. On the other side, the FWHM of (002) peaks are much smaller than (004) peaks that also mean that the crystallite size is very small. The crystallite size seems to be produced from a few crystal layers as low as about 100 crystals that can't agglomerate and aims to produce (002) later during the coating period.

3.2.2. SEM analysis of coating structures

Fig. 9 shows the comprehensive evaluation of SEM images by 250 nm (a), 350 nm (b), 450 nm (c) and 550 nm (d), respectively.

The superscripts of letters are seen as the transactional coating thickness measurements and morphology, as well. Fig. 9(a) shows 250 nm thickness in lateral growth of seeds of ZnO film. The rare seeds of ZnO can be seen but the lateral growth is evident on glass substrate very sharply. The thickness was measured about 240 nm ± 22 nm which is convenient with the thickness calibration of ZnO doped with a 5% N flow rate for the device. By increased thickness up to 350 nm (see Fig. 9 (b)), the growth of ZnO has also increased up to 410 nm ± 19 nm which is close to thickness adjustment but scattered more due to N doping. N

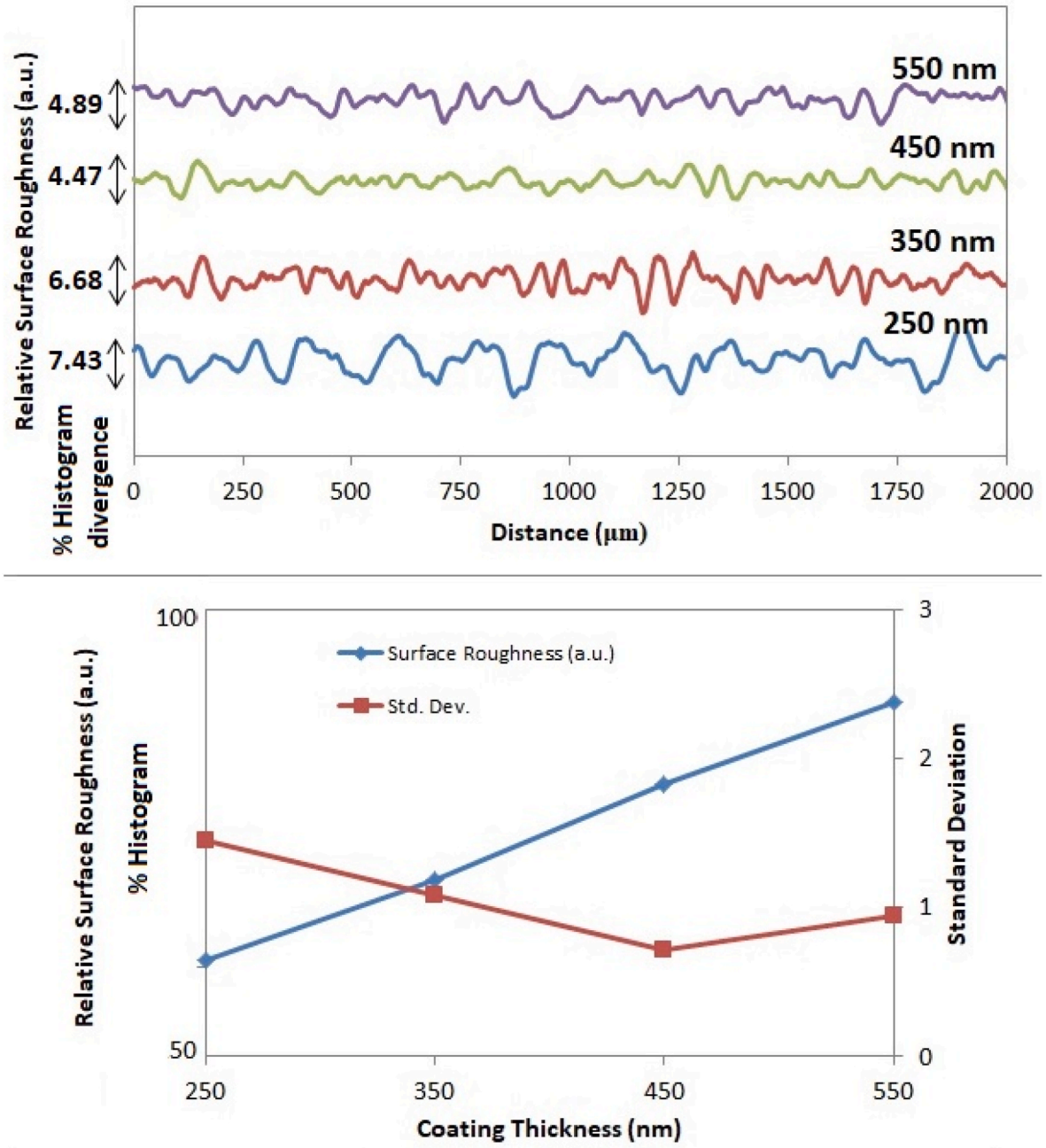

Fig. 10. Relative surface roughness values.

doping in ZnO films may also increase the thickness due to following reasons, such as;

i) The sudden pore formation on ZnO lateral seed growth due to growth rate,
ii) N interferes with Zn and O ions and scatters the O ions more due to its low atomic mass, so the NO_x precipitates to surface and then Zn deposits on them, even after NO_x/N_2, evaporates and remaining Zn is oxidized to some extent by expanding the structure as ZnO again. Besides, N doping should be considered in the center as B sites of hexagonal ZnO to expand the longitudinal axis that may increase the planar distance between c layers.

In Fig. 9(c), SEM images of surface morphology for 450 nm were given as well as thickness measurement. The thickness was measured as 520 nm ± 17 nm which is a bit higher than the adjusted thickness due to enough ZnO growth rate and regular deposition rate was achieved. With presence of N doping, N atoms along with Zn and O sputter together onto the substrate by decreased grain size. The pores were filled by increasing time and deposition thickness by stabilizing the N doping in ZnO crystal structure. For the coating in Fig. 9(d), the thickness was measured as 630 nm ± 26 nm with a high level of fluctuations due to abnormal and agglomerated growth of ZnO crystals by increased seed dimensions. By the deposition increased to a certain thickness, which is responsible for the main substrate formation, the seeds are thereafter separated onto the surface randomly which in turn may deteriorate the surface roughness and morphology after a while.

As seen by red arrows in Fig. 9(d) and **(d')**, the random distribution of seeds' deposition affects the surface by forming agglomerated and abnormal growth of the crystals; some of them are more than 100 nm. With the aid of N transfer, the ZnO deposition is carried out further up to 660 nm in some regions by producing more than 100 nm of particles in

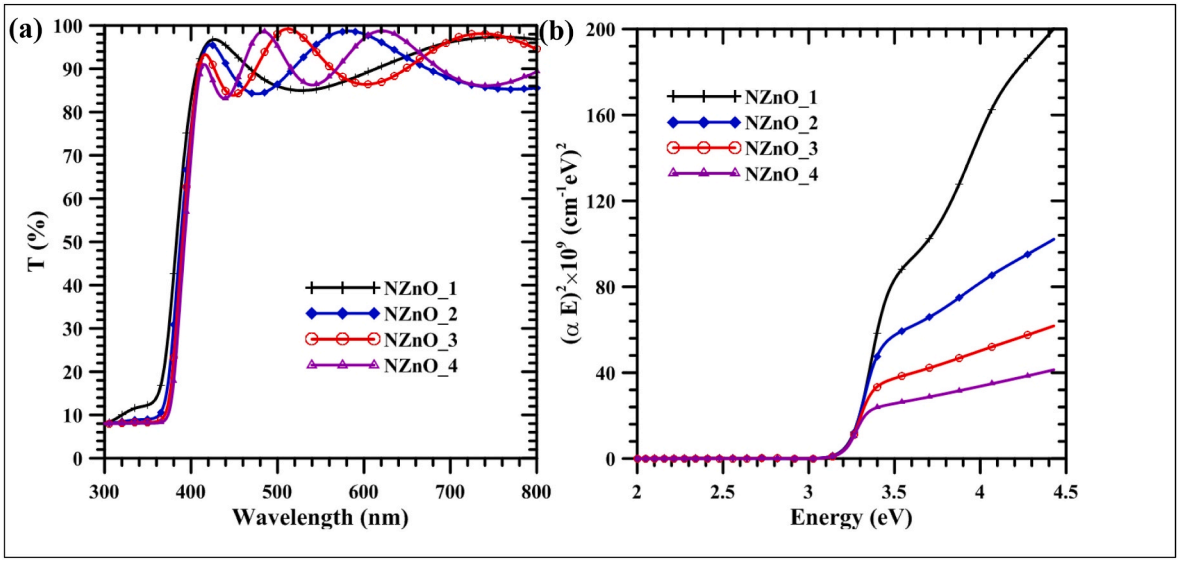

Fig. 11. a) The transmittance spectra of films for different thickness, b) Variation of $(\alpha E)^2$with photon energy of films as a function of film thickness.

the submicron range.

The SEM post-process was done for determining the relative surface roughness values of coated surfaces on the basis of coating thickness increase. Relative surface roughness is a term to correlate with image histogram to evaluate under detector to scatter more or less light than nearby pixels. Then, one can evaluate the results according to the previous one as seen in Fig. 9 by drawing a correspondence line or rectangle to take the average difference in the area. It is given in histogram % divergence for an electron if scattered from one place more or less to produce images. As seen in Fig. 10, the relative surface roughness values based on the relative histogram differences among the area of interest decrease by increasing coating thickness which is in good agreement with increased seed size and grown crystals. As the grown and abnormal seeds increase, the roughness increases to an extent but only the histogram scatter changes which can be attributed to observed bigger grain clusters to produce small hills. At this point, the best surface quality is obtained at 250 nm but with a high standard deviation due to the growth of ZnO seeds at different rates. This can also be attributed to the finer crystals cannot scatter the light but different orientations can produce different histogram scatters to observe the surface to be rougher. Whilst the surface roughness is increasing, the standard deviation on the surface hills and valleys decreased up to 450 nm and remained constant as 550 nm coating thickness. This can be said that, up to 450 nm thickness, all seeds are grown to some extent and after that, there is only a roughness increment and fluctuation on the surface is seen that makes the surface more scattering.

3.2.3. Optical properties

The graph of optical transmittance values of thin films obtained in different thicknesses by RF sputtering method versus wavelength is shown in Fig. 11 (a). It has been observed that the transmittance values of these four different thickness films are quite high, around 95% in the visible region (400–700 nm).

The variation of $(\alpha E)^2$for the films obtained at different thicknesses with respect to energy, as seen in Fig. 11 (b). The estimated band gaps of the films were found with the help of the points where the tangents drawn in the figure cut the x-axis. It was observed that the band gaps decreased from 3.25 eV to 3.20 eV as the thickness increased from 250 nm to 550 nm. Therefore, it can be said that the energy band gap is strongly dependent on the thickness. The red shift of the energy band gap with the increase in thickness can be expressed by the difference in grain size.

4. Conclusions

In summary, undoped and nitrogen-doped ZnO thin films were grown on silicon and glass substrates with controlling the nitrogen flow rate between 0% −12.5%. XRD analysis confirmed that the nitrogen-doped ZnO films exhibit the hexagonal crystal structure. Transmittance spectra were obtained by spectrophotometer measurements and the effect of nitrogen ratio was investigated. The band gap values were changed by changing N doping. The refractive index values of ZnO films decrease with introducing nitrogen into the structure. SEM images revealed that the grain size of the films decreased with increasing N doping. N–O, Zn–N, and Zn–N–O stretching were observed in FTIR analysis. 5% nitrogen-doped ZnO films were deposited on the glass substrate by RF magnetron sputtering method at room temperature with different thicknesses. The increase of the film thickness increases the grain size. It was observed that the band gaps decreased from 3.25 eV to 3.20 eV as the thickness increased.

Authors statement

I can confirm that the manuscript has been revised and approved by all named authors and that there are no other persons who satisfied the criteria for authorship but are not listed. I further confirm that the order of authors listed in the manuscript has been approved by all of us and all the authors have contribution to complete this manuscript.

CRediT authorship contribution statement

H. Hopoğlu: Writing – review & editing. **H.S. Aydınoğlu:** Writing – review & editing. **A. Özer:** Methodology, Writing – review & editing. **E. Şenadım Tüzemen:** Conceptualization, Methodology, Writing – review & editing, Formal analysis, Investigation, Visualization, Funding acquisition.

Declaration of competing interest

The authors declare that they have no known competing financial interests or personal relationships that could have appeared to influence the work reported in this paper.

Acknowledgements

This research was supported by Scientific Research Project Fund of

Sivas Cumhuriyet University under the project number RGD-032. The authors acknowledge the usage of the Nanophotonics Research and Application Center at Sivas Cumhuriyet University (CUNAM), Sivas Cumhuriyet University R&D Center (CUTAM), Cukurova University Department of Physics facilities.

References

[1] Z. Xia, L. Lu, J. Li, Z. Feng, S. Deng, S. Wang, H.S. Kwok, M. Wong, Characteristics of elevated-metal metal-oxide thin-film transistors based on indium-tin-zinc oxide, IEEE Electron. Device Lett. 38 (7) (2017) 894–897.
[2] M.T. Greiner, M.G. Helander, W.-M. Tang, Z.-B. Wang, J. Qiu, Z.-H. Lu, Universal energy-level alignment of molecules on metal oxides, Nat. Mater. 11 (2012) 76–81.
[3] T. Karlsson, A. Roos, Optical properties and spectral selectivity of copper oxide on stainless steel, Sol. Energy Mater. 10 (1984) 105–119.
[4] P. Kanmanı, J.-W. Rhim, Properties and characterization of bionanocomposite films prepared with various biopolymers and ZnO nanoparticles, Carbohydr. Polym. 106 (2014) 190–199.
[5] S. Jebril, H. Kuhlmann, S. Muller, C. Ronning, L. Kienle, V. Duppel, Y.K. Mishra, R. Adelung, Epitactically interpenetrated high quality ZnO nanostructured junctions on microchips grown by the vapor liquid solid method, Cryst. Growth Des. 10 (7) (2010) 2842–2846.
[6] M.L. Addonizio, A. Aronne, S. Daliento, O. Tari, E. Fanelli, P. Pernice, Sol-gel synthesis of ZnO transparent conductive films: the role of pH, Appl. Surf. Sci. 305 (2014) 194–202.
[7] B. Chakraborty, S. Chakrabarty, S. Ghosh, C.R. Chaudhuri, High performance biosensor based on RGO/ZnO thin film transistor, IEEE SENSORS (2018) 1–4.
[8] A.G.S. Kumar, L. Obulapathi, T.S. Sarmash, D.J. Rani, M. Maddaiah, T.S. Rao, K. Asokan, Structural, electrical and optical properties of Cd doped ZnO thin films by Reactive dc Magnetron Sputtering, J. Occup. Med. 67 (4) (2015) 834–839.
[9] A.A. Md Ralib, A.N. Nordin, Application of taguchi signal to noise ratio design method to ZnO thin film CMOS SAW resonators, IEEE Access 7 (2019) 27993–28000.
[10] B.G. Lewis, D.C. Paine, Applications and processing of transparent conducting oxides, MRS Bull. 25 (2000) 22–27.
[11] H. Kim, C.M. Gilmore, A. Piqué, J.S. Horwitz, H. Mattoussi, H. Murata, D. B. Chrisey, Electrical, optical, and structural properties of indium–tin–oxide thin films for organic light-emitting devices, J. Appl. Phys. 86 (11) (1999) 6451–6461.
[12] J.A.A. Selvan, A.E. Delahoy, S. Guo, Y.-M. Li, A. New light trapping TCO for nc-Si: H solar cells, Sol. Energy Mater. Sol. Cell. 90 (18) (2006) 3371–3376.
[13] F.S.S. Chien, C.R. Wang, Y.L. Chan, H.L. Lin, M.H. Chen, R.J. Wu, Fast-response ozone sensor with ZnO nanorods grown by chemical vapor deposition, Sensor. Actuator. B Chem. 144 (2010) 120–125.
[14] Ş. Ţălu, M. Bramowicz, S. Kulesza, S. Solaymani, A. Ghaderi, L. Dejam, S.M. Elahi, A. Boochani, Microstructure and micromorphology of ZnO thin films: case study on Al doping and annealing effects, Superlattice. Microst. 93 (2016) 109–121.
[15] X. Noirfalise, T. Godfroid, G. Guisbiers, R. Snyders, Synthesis of fluorine doped zinc oxide by reactive magnetron sputtering, Acta Mater. 59 (2011) 7521–7529.
[16] S.K. Mohanta, D.C. Kim, H.K. Cho, S.J. Chua, Structural and optical properties of ZnO nanorods grown by metal organic chemical vapor deposition, Cryst. Growth 310 (2008) 3208–3213.
[17] K. Ramamoorthy, C. Sanjeeviraja, M. Jayachandran, K. Sankaranarayanan, P. Misra, L.M. Kukreja, Development of a novel high optical quality ZnO thin films by PLD for III–V opto-electronic devices, Curr. Appl. Phys. 6 (2006) 103–108.
[18] L. Cao, L. Zhu, J. Jiang, R. Zhao, Z. Ye, B. Zhao, Highly transparent and conducting fluorine-doped ZnO thin films prepared by pulsed laser deposition, Sol. Energy Mater. Sol. Cells 95 (2011) 894–898.
[19] S. Boulahlib, K. Dib, M. Özacar, Y. Bessekhouad, Optical, dielectric, and transport properties of Ag-doped ZnO prepared by Aloe Vera assisted method, Opt. Mater. 113 (2021) 110889.
[20] S. Kurtaran, Al doped ZnO thin films obtained by spray pyrolysis technique: influence of different annealing time, Opt. Mater. 114 (2021) 110908.
[21] B. Al Farsi, T.M. Souier, F. Al Marzouqi, M. Al Maashani, M. Bououdina, H. M. Widatallah, M. Al Abri, Structural and optical properties of visible active photocatalytic Al doped ZnO nanostructured thin films prepared by dip coating, Opt. Mater. 113 (2021) 110868.
[22] A. Baptista, F. Silva, J. Porteiro, J. Míguez, G. Pinto, Sputtering physical vapour deposition (PVD) coatings: a critical review on process improvement and market trend demands, Coatings 8 (11) (2018) 402.
[23] Z. Wang, Q. Li, Y. Yuan, L. Yang, H. Zhang, Z. Liu, J. Ouyang, Q. Chen, N doped ZnO (N:ZnO) film prepared by reactive HiPIMS deposition technique, AIP Adv. 10 (2020), 035122.
[24] T. Dixit, A. Kumar, I.A. Palani, V. Singh, Surface-plasmon-mediated red and near infrared emission from Au-coated ZnO/ZnCr2O4 nanocomposites, Scripta Mater. 114 (2016) 84–87.
[25] M. Navaneethan, J. Archana, Y. Hayakawa, Morphological evolution of monodispersed ZnO nanorods to 3 dimensional hierarchical flowers by hydrothermal growth, CrystEngComm 15 (2013) 8246–8249.
[26] D. Pradhan, K.T. Leung, Vertical growth of two-dimensional zinc oxide nanostructures on ITO-coated glass: effects of deposition temperature and deposition time, J. Phys. Chem. C 112 (2008) 1357–1364.
[27] Q. Wei, G. Meng, X. An, Y. Hao, L. Zhang, Temperature-controlled growth of ZnO nanostructures: branched nanobelts and wide nanosheets, Nanotechnology 16 (2005) 2561–2566.
[28] Il Jellal, K. Nouneh, H. Toura, M. Boutamart, S. Briche, J. Naja, B. Mari Soucase, M. E. Touhami, Enhanced photocatalytic activity of supported Cu-doped ZnO nanostructures prepared by SILAR method, Opt. Mater. 111 (2021) 110669.
[29] F.A. La Porta, J. Andres, M.V.G. Vismara, C.F.O. Graeff, J.R. Sambrano, M.S. Li, J. A. Varela, E. Longo, Correlation between structural and electronic order-disorder effects and optical properties in ZnO nanocrystals, J. Mater. Chem. C 2 (2014) 10164–10174.
[30] K. Ocakoglu, S.A. Mansour, S. Yildirimcan, A.A. Al-Ghamdi, F. El-Tantawy, F. Yakuphanoglu, Microwave-assisted hydrothermal synthesis and characterization of ZnO nanorods, Spectrochim. Acta Mol. Biomol. Spectrosc. 148 (2015) 362–368.
[31] A.P. de Moura, R.C. Lima, M.L. Moreira, D.P. Volanti, J.W.M. Espinosa, M. O. Orlandi, P.S. Pizani, J.A. Varela, E. Longo, ZnO architectures synthesized by a microwaveassisted hydrothermal method and their photoluminescence properties, Solid State Ionics 181 (2010) 775–780.
[32] B. Krishnakumar, T. Imae, Chemically modified novel pamam-zno nanocomposite: synthesis, characterization and photocatalytic activity, Appl. Catal. Gen. 486 (2014) 170–175.
[33] R. Velmurugan, K. Selvam, B. Krishnakumar, M. Swaminathan, An efficient reusable and antiphotocorrosive nano ZnO for the mineralization of Reactive Orange 4 under UV-A light, Separ. Purif. Technol. 80 (2011) 119–124.
[34] C.H. Park, S.B. Zhang, S.H. Wei, Origin of p-type doping difficulty in ZnO: the impurity perspective, Phys. Rev. B 66 (2002), 073202-073203.
[35] D.G. Kim, S. Lee, D.H. Kim, G.H. Lee, M. Isshiki, Temperature dependence of the microstructure and resistivity of indium zinc oxide films deposited by direct current magnetron reactive sputtering, Thin Solid Films 516 (8) (2008) 2045–2049.
[36] K.C. Aw, Z. Tsakadze, A. Lohani, S. Mhaisalkar, Influence of radio frequency sputtering power towards the properties of indium zinc oxide semiconducting films, Scripta Mater. 60 (1) (2009) 48–51.
[37] Y.S. Jung, J.Y. Seo, D.W. Lee, D.Y. Jeon, Influence of DC magnetron sputtering parameters on the properties of amorphous indium zincoxide thin film, Thin Solid Films 445 (2003) 63–71.
[38] B.G. Choi, I.H. Kim, D. H Kim, K.S. Lee, T.S. Lee, B. Cheong, Y.-J. Baik, W.M. Kim, Electrical, optical and structural properties of transparent and conducting ZnO thin films doped with Al and F by rf magnetron sputter, J. Eur. Ceram. Soc. 25 (12) (2005) 2161–2165.
[39] M.-L. Tu, Y.-K. Su, C.-Y. Ma, Nitrogen-doped p-type ZnO films prepared from nitrogen gas radiofrequency magnetron sputtering, J. Appl. Phys. 100 (2006), 053705.
[40] X. Nie, B. Zhang, J. Wang, L. Shi, Z.F. Di, Q. Guo, Room-temperature ferromagnetism in p-type nitrogen-doped ZnO films, Mater. Lett. 161 (2015) 355–359.
[41] T. K. Pathak, R. Kumar, L. P. Purohit, Preparation and Optical properties of undoped and Nitrogen doped ZnO thin films by RF sputtering, Int. J. Chem. Res. 7 (2) (2014-2015) 987-993.
[42] R. Perumal, Z. Hassan, Effect of nitrogen doping on structural, morphological, optical and electrical properties of radio frequency magnetron sputtered zinc oxide thin films, Physica B 490 (2016) 16–20.
[43] B.D. Cullity, S.R. Stock, Elements of X-Ray Diffraction, third ed., Prentic Hall, NJ, 2001.
[44] J. Lu, Q. Zhang, J. Wang, F. Saito, M. Uchida, Powder Technol. 162 (2006) 33–37.
[45] A.B. Lavand, Y.S. Malghe, Synthesis, characterization and visible light photocatalytic activity of nitrogen-doped zinc oxide nanospheres, Journal of Asian Ceramic Societies 3 (2015) 305–310.
[46] K. Saito, Y. Hosokai, K. Nagayama, K. Ishida, K. Takahashi, M. Konagai, B.P. Zhang, J. Cryst. Growth 272 (2004) 805–809.
[47] M. Sathya, A. Claude, P. Govindasamy, K. Sudha, Growth of pure and doped ZnO thin films for solar cell applications, Adv. Appl. Sci. Res. 3 (5) (2012) 2591–2598.
[48] E. Şenadım Tüzemen, S. Eker, H. Kavak, R. Esen, Dependence of film thickness on the structural and optical properties of ZnO thin films, Appl. Surf. Sci. 255 (2009) 6195–6200.
[49] A. Hassan, Y. Jin, M. Irfan, Y. Jiang, Acceptor-modulated optical enhancements and band-gap narrowing in ZnO thin films, AIP Adv. 8 (2018), 035212.
[50] N.R. Yogamalar, A.C. Bose, Burstein–Moss shift and room temperature near-band-edge luminescence in lithium-doped zinc oxide, Appl. Phys. A 103 (1) (2011) 33–42.
[51] S. Mobtakeri, Y. Akaltun, A. Özer, M. Kılıç, E. Şenadım Tüzemen, E. Gür, Gallium oxide films deposition by RF magnetron sputtering; a detailed analysis on the effects of deposition pressure and sputtering power and annealing, Ceram. Int. 47 (2021) 1721–1727.
[52] Y. Liao, S. Jiao, S. Li, J. Wang, D. Wang, S. Gao, Q. Yu, H. Li, Effect of deposition pressure on the structural and optical properties of Ga2O3 films obtained by thermal post-crystallization, Cryst. Eng. 20 (2018) 133–139.
[53] C.V. Ramana, E.J. Rubio, C.D. Barraza, A.M. Gallardo, S.A. McPeak, S. Kotru, J. T. Grant, Chemical bonding, optical constants, and electrical resistivity of sputter-deposited gallium oxide thin films, J. Appl. Phys. 115 (2014), 043508.